High-Dispersion Spectroscopy of the X-Ray Transient RXTE J0421+560 (= CI Cam) during Outburst[1]

Edward L. Robinson, Inese I. Ivans, and William F. Welsh[2]

Department of Astronomy, The University of Texas, Austin, TX 78712

ABSTRACT

We obtained high dispersion spectroscopy of CI Cam, the optical counterpart of XTE J0421+560, two weeks after the peak of its short outburst in 1998 April. The optical counterpart is a supergiant B[e] star that is emitting a two-component wind, a cool, low-velocity wind and a hot, high-velocity wind. The cool wind, which is the source of narrow emission lines of neutral and ionized metals, has a velocity of 32 km s^{-1} and a temperature near 8000 K. It is dense, roughly spherical, fills the space around the sgB[e] star, and, based on the size of an infrared-emitting dust shell around the system, extends to a radius between 13 AU and 50 AU. It carries away mass at a high rate, $\dot{M} > 10^{-6}\ M_\odot$ yr^{-1}. The hot wind has a velocity in excess of 2500 km s^{-1} and a temperature of $1.7 \pm 0.3 \times 10^4\ K$. From an ultraviolet spectrogram of CI Cam obtained in 2000 March with Hubble Space Telescope, we derive a differential extinction $E(B-V) = 0.85 \pm 0.05$.

We show that the distance to CI Cam is greater than 5 kpc. Based on this revised distance, the X-ray luminosity at the peak of the outburst was $L(2-25\text{ keV}) > 3.0 \times 10^{38}$ erg s^{-1}, making CI Cam one of the most luminous X-ray transients. The ratio of quiescent luminosity to peak luminosity in the $2-25$ keV band is $L_q/L_p < 1.7 \times 10^{-6}$.

The compact star in CI Cam is immersed in the dense circumstellar wind from the sgB[e] star and burrows through the wind producing little X-ray emission except for rare transient outbursts. This picture, a compact star traveling in a wide orbit through the dense circumstellar envelope of a sgB[e] star, occasionally producing transient X-ray outbursts, makes CI Cam unique among the known X-ray binaries. There is strong circumstantial evidence that the compact object is a black hole, not a neutron star. We speculate that the X-ray outburst was short because the accretion disk around the compact star is fed from a stellar wind and is smaller than disks fed by Roche-lobe overflow.

Subject headings: binaries: close — stars: emission-line, Be — stars: individual (CI Cam, RXTE J0421+560) — stars: winds, outflows — X-rays: binaries

1. I. Introduction

The outburst of the transient X-ray source XTE J0421+560 began 1998 March 31.6 UTC and peaked only $\sim$ 12 hours later at nearly 1.9 crab (2 - 10 keV). The outburst faded rapidly, initially on an e-folding time scale of 0.6 days and then slowing to a time scale of 2.3 days, reaching quiescence in less than two weeks (Belloni et al. 1999). There were no coherent pulsations in the X-ray light curve with amplitudes greater than 0.1% rms at frequencies between 0.01 and 4096 Hz, nor quasi-periodic oscillations with amplitudes greater than 0.7%. The outburst was also detected by the PCA on RXTE, and by BATSE,

[1]Based on observations made with the NASA/ESA Hubble Space Telescope, otained at the Space Telescope Science Institute, which is operated by the Association of Universities for Research in Astronomy, Inc., under NASA contract NAS 5-26555.

[2]Current address: Department of Astronomy, San Diego State University, 5500 Campanile Dr., San Diego, CA 92182

BeppoSAX, and ASCA at energies from 0.3 to 75 keV (Frontera et al. 1998; Harmon et al. 1998; Paciesas & Fishman 1998; Ueda et al. 1998; Belloni et al. 1999). The flux distribution at energies greater than 1 keV was consistent with either a two-temperature thermal bremsstrahlung spectrum (1.1 and 5.7 keV) or a power law with a high-energy cutoff; the spectrum softened as CI Cam faded towards quiescence. In addition, there was an extremely soft component confined to energies less than 1 keV that appeared only during two short flares (Ueda et al. 1998). Weak X-ray emission was also detected in quiescence, 157 days after the outburst (Orlandini et al. 2000).

The optical counterpart to J0421+560 is CI Cam (= MWC 84 = MW 143) (Smith & Remillard 1998; Hjellming & Mioduszeswki 1998a; Wagner & Starrfield 1998; Robinson et al. 1998). Before its outburst CI Cam was a low-amplitude, irregular variable star with $<V> = 11.6$. There was no convincing pattern to its variations (Bergner et al. 1995), although Miroshnichenko (1995) has suggested that the variations showed an 11.7 d quasi-period. The pre-outburst spectrum of CI Cam had strong, broad emission lines of H and He I, and narrow emission lines of Fe II, all superimposed on a hot, blue continuum; there were no absorption lines, nor were there emission lines from highly ionized species such as He II and [O III] (Downes 1984). The spectrum was not noticeably different in spectrograms taken as early as 1931 (Merrill 1933). Allen (1973) found a strong infrared excess, which he attributed to thermal emission from circumstellar dust with temperatures between 1190 and 1350 K. According to Zorec (1998), the distance to CI Cam is 1750 pc and its luminosity is $M_{bol} = -6.9$.

These properties clearly place CI Cam among the supergiant B[e] stars (Zickgraf 1998; Miroshnichenko 1998; Lamers et al. 1998). The sgB[e] stars are massive, evolved, high-luminosity stars undergoing mass loss in a two-component wind. The rates of mass loss are prodigious, typically greater than 10^{-5} $M_\odot$ yr^{-1} (Pacheco 1998). The notation "B[e]" or "sgB[e]" risks confusing these stars with the ordinary Be stars, which are rapidly rotating stars near the main sequence losing mass in an equatorial wind. In practice, however, the spectroscopic and photometric properties of the sgB[e] stars are easily distinguished from those of Be stars.

The optical, infrared, and radio light curves of the 1998 outburst have been collected together by Clark et al. (2000). CI Cam rose by at least 3.4 magnitudes in the R band, reaching $R \approx 7.1$, and then faded towards quiescence, initially on an e-folding time scale of 3.4±0.4 days and then slowing to an e-folding time of ~ 24 days a few weeks after the outburst peak. Although the optical flux soon returned to its quiescent level, the near-infrared flux remained $\sim$ 0.5 magnitudes above the pre-outburst flux for at least one year after the outburst, which led Clark et al. (2000) to infer that either the structure or composition of the dust shell had changed. The radio light curves were consistent with synchrotron emission from an expanding cloud. VLA maps suggested that CI Cam ejected relativistic corkscrew jets during the outburst but the jets have not been confirmed by other observations (Hjellming & Mioduszeswki 1998b).

The equivalent widths of the emission lines in the optical spectrum of CI Cam increased substantially during the outburst. The He I line at 6876 Å reached almost 400 Å before dropping back to ∼50 Å in quiescence, and the 4686 Å line of He II appeared in emission and grew to an equivalent width of $\sim$ 70 Å before fading to $<$ 2 Å 40 days later (Barsukova et al. 1998). The Na I D lines, invisible in quiescence, reached an equivalent width near 40 Å. By early 1999, 10 months after the outburst, the optical spectrum was again similar to the pre-outburst spectrum (Orlandini et al. 2000).

The outburst of J0421+560/CI Cam was unusually short for an X-ray transient and, accepting for the moment the distance given by Zorec (1998), its luminosity was rather low, a few times 10^{37} ergs s^{-1}. This suggested to Belloni et al. (1999) that CI Cam is similar to A0538-66, an X-ray binary containing an ordinary Be star and a neutron star. The neutron star in A0538-66 has a rotation period of 0.067 s, an orbital period of 16.65 days, and an orbital eccentricity greater than 0.8 (Bildsten et al. 1997). The system has transient X-ray outbursts that recur at multiples of the orbital period, presumably when the neutron star passes through the equatorial wind from the Be star. The X-ray outbursts have durations between a few hours and 10 days and luminosities

from $\sim 10^{37}$ to 10^{39} erg s^{-1}, but the outbursts can disappear altogether for many years, possibly because the equatorial wind is strongly variable (Corbet et al. 1997).

In this paper we present high-dispersion, optical spectroscopy of CI Cam obtained two weeks after the peak of the 1998 outburst, and ultraviolet spectroscopy obtained with HST in 2000 March. We use the data to investigate the structure of the CI Cam system and elucidate the nature of the X-ray transient.

2. Observations

2.1. Optical Spectroscopy and Line Identifications

We measured the spectrum of CI Cam on 1998 April 14, 15 and 17 UTC with the coudé echelle spectrograph of the 2.7-m telescope at McDonald Observatory (Tull et al. 1995). The spectrograms have a resolution of R = 60,000 and a useful spectral range from ~4300 Å to 1.02 μm except for inter-order gaps at longer wavelengths. We observed CI Cam for ~1.5 hours each night before it set in the west, obtaining three or four individual exposures of 15 – 30 minutes each night. Although these spectra were obtained only two weeks after the beginning of the outburst, CI Cam had already faded to within 0.5 mag of minimum light and its brightness was no longer changing rapidly.

There are no absorption lines in the visual spectrum of CI Cam other than interstellar absorption features but, in compensation, CI Cam has a rich emission-line spectrum. Some of the lines are extraordinarily strong: Hα had an equivalent width of ~750 Å, the O I line at 8446 Å had an equivalent width of ~175 Å, and the He I triplet line at 7065 Å had an equivalent width of ~145 Å. The list of species for which we have certain identifications is given in Table 1. The identifications are conservative and were accepted only if supported by several emission lines.

None of the emission lines showed detectable radial velocity variations during the observations. The upper limit to the variations is ± 0.5 km s^{-1} except for the He II lines, for which the upper limit is ± 1.5 km s^{-1}. The He II line at 4686 Å is contaminated by an instrumental artifact and the He II line at 10123 Å line is contaminated by OH emission from the night sky (Osterbrock et al 1997), so we exclude He II from further discussion.

The heliocentric radial velocities of individual species run from -42.6 km s^{-1} for [N II] to -46.4 km s^{-1} for the Paschen lines, but we consider the differences among these velocities to be the upper limit to any real differences because the profiles of the emission lines vary from species to species. The mean radial velocity for all species we measured is -44.4 ± 0.6 km s^{-1}, where the standard deviation refers to statistical errors; systematic errors introduced by the asymmetric line profiles could be several times larger. The radial velocity with respect to the Local Standard of Rest is -51 km s^{-1}.

Figure 1 shows the region of the spectrum near 5860 Å. The upper panel shows the strongly asymmetric He I line at 5876 Å and the Na D lines at 5890/96 Å (dissected by narrow interstellar absorption lines), and the lower panel shows the same portion of the spectrum magnified vertically to show the wings of the helium line and also the weaker lines in the spectrum. The blue wing of the He I line extends to at least 5845 Å (-1500 km s^{-1}); the maximum extent of the red wing is uncertain because of the overlapping Na D lines. The weak absorption feature at 5850 Å is a diffuse interstellar band (Krełowski & Schmidt 1997).

The thicket of weak emission lines seen in the blue wing of He I 5876 Å extends throughout the optical spectrum. Figure 2 shows the region of the spectrum near 5160 Å and provides identifications for the stronger lines. Most of the lines come from Fe II but many come from Ti II and Mg I. Forbidden Fe II lines are present throughout the spectrum (e.g., $\lambda\lambda$ 5158.00/5158.81 Å) but they are generally much weaker than the permitted Fe II lines.

Figure 3 shows the portion of the infrared spectrum of CI Cam containing the O I line at 8446 Å, some members of the hydrogen Paschen series, some Fe I lines, and the Ca II 8498 Å line – a member of the Ca II infrared triplet. The Paschen lines can be traced to P34 in other orders of the spectrogram. The O I line at 8446 Å is particularly interesting because it can be enhanced by resonance-fluorescence (Grandi 1975; Kastner & Bhatia 1995). The strongest transition of the $2p^4\,{}^3P - 3d\,{}^3D^0$ multiplet (UV 4) of O I has a wavelength of 1025.77 Å. O I atoms in the ground

state can absorb Lyβ photons at 1025.72 Å and then electrons in the 3d ^{3}D° level can branch to the 3p ^{3}P level, emitting a photon at 11287 Å followed by one at 8446 Å.

Figure 4 shows another portion of the infrared spectrum, with the N I lines from multiplets 1 and 8, some Paschen lines, more Fe I and [Fe II] lines, and Ca II 8662 Å – another member of the infrared triplet.

2.2. Ultraviolet Observations and Reddening

We derived the reddening of CI Cam from an ultraviolet spectrogram obtained with the Space Telescope Imaging Spectrograph on the Hubble Space Telescope on 20 March 2000, two years after the outburst. A more complete discussion of spectrum will be given elsewhere; here we use the spectrum only to extract the ultraviolet and optical extinction.

The spectrum was observed with the MAMA detector and the medium-resolution echelle gratings E140M in the far ultraviolet (1150 Å – 1730 Å) and E230M in the near ultraviolet (1870 Å – 2700 Å). To define the continuum distribution more accurately we rebinned the two spectrograms into 15 Å bins in the short wavelength region and 20 Å bins in the long wavelength region. The rebinned spectrograms are shown in the lower panel of Figure 5; the deep, broad dip at 2200 Å shows that the spectrum of CI Cam is heavily reddened.

We adopted the extinction law given by Cardelli et al. (1989), which has two parameters: A_V and R_V [$= A_V/E(B-V)$], where A_V is the visual extinction and $E(B-V)$ is the differential extinction between the B and V bands. We de-extincted the spectrum of CI Cam by requiring the de-extincted spectrum to match the spectral distribution of the HST standard star BD+33°2642 between 1250 Å and 2650 Å. We chose BD+33°2642 because it is a hot subgiant (spectral type B3 IV) and is likely to have a continuum spectral distribution similar to that of CI Cam. The reddening of BD+33°2642 is low but not zero: According to Tobin (1985) its reddening is $E(B-V) \sim E(b-y) = 0.011$, while Napiwotzki (1993) finds $E(B-V) = 0.06$. We have, therefore, applied a correction of 0.03 to the value of $E(B-V)$ derived from the fit, and a correction of 0.1 to A_V. We do not attempt to separate circumstellar from interstellar extinction.

The results of the fit, including the after-the-fit corrections to $E(B-V)$ and A_V, are

$$\begin{aligned} A_V &= 2.3 \pm 0.3 \\ R_V &= 2.7 \pm 0.2 \\ E(B-V) &= 0.85 \pm 0.05 \end{aligned} \tag{1}$$

The quoted errors include the uncertainty in the reddening for BD+33°2642. The values of A_V and R_V derived from the fit are strongly correlated, which increases their estimated error significantly. The de-extincted spectrum of CI Cam is shown in the upper panel of Figure 5, with the spectrum of BD+33°2642 overplotted for comparison. The fit of the de-extincted spectrum of CI Cam to the spectrum of BD+33°2642 is quite good. The high points between 2300 Å and 2500 Å, the high point near 1900 Å, and the various dips between 1200 Å and 1700 Å are all due to real features in the CI Cam spectrum: Fe II emission between 2300 Å and 2500 Å and wind features at the shorter wavelengths, for example. The value of R_V derived from our data is significantly lower than the commonly accepted value of 3.1, but the variance of the fit increases by more than a factor of two if R_V is increased from 2.7 to 3.1 and the fit looks markedly worse to the eye. The derived reddening does depend on the use of BD+33°2642 as a reddening template, but the dependence is not strong. Furthermore, $R_V = 2.7$ is well within the range of measured values for individual stars (Cardelli et al. 1989).

Belloni et al. (1999) estimated the extinction and reddening of CI Cam in quiescence from the slope of the optical/infrared continuum, finding $A_V = 4.4 \pm 0.2$, $R_V = 3.7 \pm 0.1$, and $\mathrm{E(B-V)} = 1.18 \pm 0.04$. The estimates by Zorec (1998) agree fairly well with these numbers. We attribute the difference between their values and ours to the substantial difficulties in deriving an accurate reddening from the slope of the optical continuum in an unusual star like CI Cam. Clark et al. (2000) derived $E(B-V) = 0.65 \pm 0.2$ from the strength of the diffuse interstellar bands in the optical spectrum, in rough agreement with our results. The extinction at soft X-ray wavelengths yielded $N_H = 3.76 \pm 0.36 \times 10^{22}$ cm^{-2} near the peak of the X-ray outburst, but N_H rapidly decreased to less than about 0.2×10^{22} cm^{-2} as CI Cam approached

quiescence Belloni et al. (1999). If we were to adopt $N_H/A_V = 1.79 \times 10^{21}$ atoms cm^{-2} mag^{-1}, a typical value for the interstellar medium (e.g., Predehl & Schmitt 1995), the visual extinction would be only 1.1 mag during quiescence. The ratio of optical to X-ray extinction is, therefore, higher than normal.

The change in the infrared flux after the outburst and the rapid change of the soft X-ray extinction during the outburst (Clark et al. 2000; Belloni et al. 1999), demonstrate that much of the extinction to CI Cam is local, not interstellar, raising a concern that the reddening measured from the ultraviolet spectrum in 2000 March may not be the same as the visual reddening in 1998 April. Because of this concern, most of the calculations we present later in this paper will include a much wider range of values for $E(B-V)$ than permitted by the standard deviations given in equation 1.

2.3. The Distance to CI Cam

Although the spectrum of CI Cam clearly places it among the sgB[e] stars, the sgB[e] stars are a diverse group with a wide range of luminosities (Zickgraf 1998). Zorec (1998), Belloni et al. (1999), Clark et al. (2000) and Orlandini et al. (2000) have all argued that CI Cam is located at a distance of ~ 2 kpc and has a luminosity in the range $10^{4.7} - 10^{4.9}\ L_\odot$. We argue here that CI Cam is more distant and more luminous than these estimates.

Clark et al. (2000) and others estimated the distance to CI Cam from its optical continuum extinction and from the strength of the diffuse interstellar bands. The extinction can be converted to distance using, for example, the extinction/distance graphs in Neckel et al. (1980). The extinction in the direction of CI Cam is, however, patchy and sparsely measured, so the extinction/distance relation is not well determined. In fact, the line of sight to CI Cam passes through a relatively clear window between molecular clouds, making any mean extinction/distance relation inapplicable (Dame et al. 1987). Also, CI Cam lies at a galactic latitude of $4^\circ\!.1$, well above the midplane of the galaxy as defined by the neutral hydrogen layer in that direction (Kerr et al. 1986). The line of sight to CI Cam rises to 150 pc above the plane of the galaxy at a distance of $\sim$2 kpc. Beyond this distance the line of sight exits the densest absorbing layer and encounters little further extinction until, at distances greater than ~ 5 kpc, the line of sight begins to re-enter the greatly-warped outer disk of the galaxy. Interstellar extinction gives, then, only a lower limit for the distance to CI Cam – and not a particularly reliable one.

Belloni et al. (1999) show that CI Cam must be more distant than 350 pc and then simply assign CI Cam to the Perseus arm, which is at a distance of $\sim$2 kpc. H II regions and young clusters are not, however, strongly confined to the Perseus arm in the direction of CI Cam and some are found many kiloparsecs beyond the Perseus arm (Taylor & Cordes 1993), so the argument for placing CI Cam in the Perseus arm is not strong. The distance determinations by Zorec (1998) rely on uncertain measurements and relationships, and could easily be in error by large factors for individual stars.

Two lines of evidence show that CI Cam is much more distant than 2 kpc. The first is based on the spectrum of CI Cam. Although helium lines are present in the spectra of most sgB[e] stars, the lines are often present in absorption, not emission; and, even when in emission, they are generally much weaker than the helium emission lines in the spectrum of CI Cam (Jaschek 1998). The supergiant B[e] star Hen S 134 does have strong He I emission lines and its spectrum is strikingly similar to that of CI Cam. [Compare the quiescent spectra of CI Cam in Downes (1984) and Orlandini et al. (2000) to the spectrum of Hen S 134 in Zickgraf et al. (1986).] Hen S 134 is extremely luminous. Even though it is in the LMC, its visual magnitude is $V \approx 12.0$. The de-extincted visual magnitude of CI Cam is $V \approx 9.3$, so if CI Cam is as luminous as Hen S 134, its distance is greater than 10 kpc.

Also, as we will show in the next section, the Fe II emission lines in the spectrum of CI Cam, which arise in a circumstellar wind from the sgB[e] star, have a half width at half maximum (HWHM) of only 32 km s^{-1}. The HWHMs of the Fe II emission lines in most other sgB[e] stars are typically 50 – 75 km s^{-1} or more (Oudmaijer et al. 1998). The notable exceptions are, once again, the extremely luminous supergiant B[e] stars: The Fe II lines have a HWHM of 36 km s^{-1} in Hen S 134 and 20 km s^{-1} in the sgB[e] star R126 (Zickgraf

et al. 1985, 1986). Since wind velocities tend to be strongly correlated with the surface gravities of the emitting stars, the low velocity of the wind from CI Cam again places it among the largest and most luminous sgB[e] stars.

The second line of evidence is based on the structure of the Galaxy. The radial velocity of CI Cam with respect to the Local Standard of Rest is -51 km s^{-1} and its galactic longitude and latitude are $(l,\ b) \approx (149°,\ 4°)$. Since CI Cam is a young, extreme Population I object, it should lie close to the plane of the galaxy and have a nearly circular orbit around the galactic center. If we assume that its radial velocity is produced by differential galactic rotation and use typical models for the galactic rotation (Burton 1988a), its distance is ~ 7 kpc. Also, for any distances between 2 and 6 kpc, the galactic latitude of CI Cam places it several hundred parsecs above the plane of the galaxy, much higher than expected for young objects. However, the outer disk of the galaxy begins to warp upwards in the direction of CI Cam at distances greater than a few kiloparsecs, and at distances beyond 7 kpc the line of sight to CI Cam again penetrates the galactic disk (Burton 1988b). Thus the galactic latitude of CI Cam implies distances approaching 7 kpc.

Finally, the known H II regions with angular separations from CI Cam less than 5° have distances between ~ 0.9 and ~ 9.0 kpc (Blitz et al. 1982; Chan & Fich 1995). CI Cam could reasonably lie at any distance up to ~ 9.0 kpc.

For the purposes of this paper, it is sufficient to place CI Cam at 5 kpc, 2.5 times further than previously supposed, but we emphasize that this is likely to be a lower limit to the true distance.

2.4. The X-ray Luminosity of CI Cam

According to Belloni et al. (1999) the unabsorbed 2 – 25 keV flux from CI Cam at the peak of its outburst was $\sim 1.1 \times 10^{-8}$ erg cm^{-2} s^{-1}. At the revised distance, its X-ray luminosity becomes

$$L(2 - 25 \text{ keV}) \ \approx\ 3.0 \times 10^{38} \left(\frac{\text{d}}{5 \text{ kpc}}\right)^2 \text{ erg s}^{-1} \tag{2}$$

This luminosity lies near the upper end of the range of peak luminosities for X-ray transients and is greater than the luminosity of most of the black hole X-ray transients (Chen et al. 1997). CI Cam was, therefore, a high-luminosity X-ray transient.

Using the quiescent hard X-ray flux measured by Orlandini et al. (2000), we find the quiescent hard X-ray luminosity of CI Cam to be

$$L(2 - 10 \text{ keV}) \ =\ 5.0 \times 10^{32} \left(\frac{\text{d}}{5 \text{ kpc}}\right)^2 \text{ erg s}^{-1}. \tag{3}$$

Fits to the X-ray spectrum of CI Cam in quiescence required a second, extremely-soft, thermal bremsstrahlung component (kT $= 0.22 \pm 0.8$ keV) with an unabsorbed luminosity of 2×10^{34} ergs s$^{-1}(d/5\text{ kpc})^2$ in the 0.5 – 2.0 keV band (Orlandini et al. 2000). While X-ray transients often display a soft X-ray excess during outbursts, the excess is never this soft and never present during quiescence. We suspect this soft component is produced by the wind from the sgB[e] star and is not directly associated with the compact object in CI Cam. Most high-luminosity OB stars are intrinsic X-ray sources and their X-ray luminosity is strongly correlated with their bolometric luminosity and with the rate at which kinetic energy is carried away by their stellar winds. According to Sciortino et al. (1990), their X-ray luminosity in the 0.2 - 4.0 keV band is related to their bolometric luminosity by

$$\log L_x \ =\ 1.08^{+0.06}_{-0.22} \log L_{bol} - 9.38^{+2.32}_{-0.83}. \tag{4}$$

The bolometric luminosities of the sgB[e] stars range from $\log(L_{bol}/L_\odot) = 5.0$ to 6.0 (Zickgraf 1998). For $\log(L_{bol}/L_\odot) = 5.5$ this relation allows X-ray luminosities approaching 10^{34} ergs s^{-1}, so most of the quiescent X-ray flux from CI Cam could be coming from the sgB[e] star. Orlandini et al. (2000) concluded that the quiescent X-ray flux cannot come from the sgB[e] star. Our conclusion differs from theirs because we have adopted a higher bolometric luminosity for CI Cam and have used a more modern relation between L_x and L_{bol}.

Some of the flux from this extremely soft component in CI Cam may contribute to the flux in the 2.0 - 10 keV band and, therefore, the quiescent flux observed in the 2.0 - 10 keV band is an upper limit to the flux in that band from the compact star alone. The ratio of quiescent luminosity to peak luminosity for the entire CI Cam system is $L_q/L_p \sim 1.7 \times 10^{-6}$, independent of distance, but for the compact star alone, the ratio is $L_q/L_p < 1.7 \times 10^{-6}$.

3. The Kinematic Properties of the Circumstellar Environment

The great range of the widths and profiles of the emission lines in the spectrum of CI Cam, and the range of ionization states of the emitting species implies that the circumstellar environment of CI Cam is kinematically and thermally complex. There are three kinematically distinct regions. The first region is the source of the narrow, symmetric lines of [N II] and [O III], the second is the source of the metal lines and the hydrogen Paschen lines, and the third is the source of the extremely broad lines of H, He I, and Na D. The properties of the regions are summarized in Table 2.

Region I: The first region is characterized by emission lines with a HWHM near 17 km s^{-1}. It is the source of the highly-forbidden emission lines of [O III] at 4363 Å, 4959 Å, and 5007 Å; and of [N II] at 5755 Å and 6583 Å (the 6548 Å line of [N II] is hidden in the strong, steeply-sloped blue wing of Hα). Figure 6 shows the [O III] line at 5007 Å and the [N II] line at 5755 Å. The [O III] lines have a nearly Gaussian profile with a HWHM of 16.4 km s^{-1}. The [N II] line at 5755 Å has two components, a narrow component with a Gaussian profile and a HWHM of 17.2 km s^{-1} and a broad component with a HWHM of 190 km s^{-1}. The broad component is displaced 15 km s^{-1} to the blue of the narrow component, causing the asymmetric line wings. Only the narrow component is clearly visible in the [N II] 6583 Å line. The radial velocities of the [O III] lines and the narrow component of the [N II] lines are the same to within the measurement error and their mean is -43.2 km s^{-1}. No other lines in the optical spectrum, forbidden or otherwise, have similar kinematic properties.

Region II: The second region is characterized by emission lines with HWHM between 32 and 35 km s^{-1}. This region is the source of all the permitted lines except for the Balmer lines, the helium lines, and the Na D lines. It is also the source of the [Fe II] and [O I] forbidden lines and of most of the emission in the higher members of the Paschen series. The profiles of the weaker metal lines are nearly rectangular. The stronger lines have more rounded profiles, becoming almost Gaussian in shape as the lines become stronger, and the very strongest lines have an extended blue wing. The [Fe II] lines are nearly rectangular but have a dip in the middle of their profiles.

We fit the emission lines in a portion of the spectrum between 5415 Å and 5436 Å with a model in which the lines are the convolution of a rectangular line profile that has the same width for all lines, and a broadening profile that can be different for different lines. The physical picture behind this model is a spherically-symmetric, uniformly-expanding wind that is optically thin in the continuum and produces emission lines. The bulk motion of the wind gives an identical underlying rectangular profile to all the lines. In addition, each line has its own local line profile. The local line profiles all include a narrow Gaussian component, which is slightly wider for stronger lines than weaker lines; and the profiles of the stronger lines have a second, broad Gaussian component to model their broad, asymmetric wings. The convolution corresponds to a simple sum of the local line profiles over the volume of the wind.

The fit of the model to the data, shown in Figure 7, is excellent considering the model's simplicity. The half width of the rectangular line profile is 0.58 Å. The 1-σ width of the narrow Gaussian component is 0.072 Å for the four weakest lines and 0.117 Å for the two strongest lines. Broad Gaussian wings were needed for the three Fe II lines but were not needed for the Fe I, Ti II, and Cr II lines. The width and displacement of the broad Gaussian component increased with increasing line strength.

The expansion velocity of the wind, which we will call the "iron wind," is given by the half width of the rectangular profile, 32 km s^{-1}. After a small correction for broadening in the spectrograph, the width of the narrow Gaussian component in the four weakest lines is 3.1 km s^{-1}, and, notably, its width is the same in the Ti II 5418 Å and the Cr II 5421 Å lines even though they differ in strength by a factor of 2.2. Since the widths and profiles of the weaker lines are independent of their strength, the profiles are dominated by kinematics, not radiative transfer. In contrast, the profiles of the stronger Fe II lines do depend on line strength, so their profiles are affected by radiative transfer.

The iron wind is remarkably uniform. The rect-

angular profiles of the weaker lines, which are the best tracers of the wind geometry and kinematics, allow little deviation from a spherically symmetric geometry and, in particular, there cannot have been any large gaps in the wind. There is no evidence that the iron wind rotates. The projected rotational broadening of the lines must be a small fraction ($\lesssim$10%) of the expansion velocity to avoid producing the double peaks and broad line wings that are typical markers of rotation. We will show in the next section that the width of the narrow Gaussian component is due primarily to thermal broadening. Thus, there is little turbulence and little radial acceleration or deceleration in the wind.

Region III: The third region is characterized by emission lines with a HWHM greater than 50 km s^{-1} and is the source of the Balmer lines, the He I lines, and the Na D lines (see Figures 1 and 8). All these lines have broad, asymmetric wings and large equivalent widths. The He I 6678 Å line and Hβ are relatively uncontaminated by other lines; we modeled them with two Gaussian components: The line cores required Gaussians with a HWHM of $\sim$ 60 km s^{-1} for Hβ and $\sim$ 50 km s^{-1} for He I; and the broad wings of both lines required Gaussians with a HWHM of $\sim$ 160 km s^{-1} displaced by $\sim$ 60 km s^{-1} to the blue. Although a two-Gaussian fit does seem to work for all the lines arising in this region, the widths of the Gaussians differ from line to line. For example, the HWHM of the lines in the Balmer series decrease from $\sim$ 85 km s^{-1} at Hα to $\sim$ 50 km s^{-1} at Hγ.

The full extent of the broad wings is difficult to measure because the wings are overlaid by the thicket of weak emission lines, but Hα is so broad that it extends over more than one echelle order and its blue wing extends to at least 6510 Å or -2500 km s^{-1}. The wings of Hβ extend from at least 4848 to 4872 Å or -800 to $+670$ km s^{-1}. The strong variation of the line widths and profiles with order in the Balmer series suggests that the lines are strongly affected by radiative transfer.

The broad Balmer and the helium lines most likely come from high velocity outflow but our data place only weak constraints on the the geometry of the outflow. None of the emission lines in the visual and near-infrared region have P-Cygni profiles, suggesting that the outflow is non-spherical and directed away from the line of sight. On the other hand, the C IV 1549 Å and Si IV 1394,1403 Å lines seen our *HST* spectrum of CI Cam do have pronounced P-Cygni profiles with absorption wings extending to ~ -1000 km s^{-1}, suggesting a more spherical outflow. Ikeda et al. (2000) obtained spectropolarimetry of CI Cam on 1998 April 4, 10, and 11, only a few days before we obtained our optical data. The polarization at that time was entirely consistent with interstellar polarization. There was no evidence for intrinsic continuum polarization nor did the polarization change with wavelength over the profiles of the strong emission lines, again suggesting a more spherical geometry. The data, then, slightly favor a weakly collimated outflow – a high velocity wind – rather than a purely spherical outflow or a narrowly collimated jet. The velocity of the outflow is likely to be somewhat larger than 2500 km s^{-1}, the maximum observed velocity.

4. The Thermal Properties of the Circumstellar Environment

There are four thermally distinguishable regions around CI Cam. Each of the three kinematic regions identified in the previous section has distinct thermal properties. The fourth region is the source of the infrared dust emission.

Region I: This region is the source of the highly forbidden [N II] and [O III] lines. Since the spectrograms of CI Cam are not flux calibrated, we were forced to measure the fluxes in these lines (and all other lines) indirectly, by first measuring their equivalent widths and then using Johnson BVR magnitudes to calibrate the continuum. All flux ratios were corrected for reddening. The best estimate of the reddening is the one we have derived from the ultraviolet extinction, $E(B-V) = 0.85 \pm 0.05$, but we have also calculated line flux ratios for $E(B-V) = 0.65$ and $E(B-V) = 1.1$ to include possible effects of non-standard optical reddening. There were many complications measuring the [N II] lines. The 6583 Å line is difficult to measure because it lies in the strong and steeply-sloped red wing of Hα; the 6548 Å line is lost in the blue wing of Hα, forcing us to deduce its flux from the flux in the 6583 Å line and the ratio of the transition probabilities of the two

lines; and the flux in the narrow component of the 5755 Å line had to be deconvolved from the flux in the broad component. Because of all these complications, the measured diagnostic line ratios have large uncertainties:

$$\text{[N II]:} \qquad 0.47 \leq \frac{I(6548)+I(6583)}{I(5755)} \leq 0.76 \qquad (5)$$

$$\text{[O III]:} \qquad 5.4 \leq \frac{I(4959)+I(5007)}{I(4363)} \leq 7.1 \qquad (6)$$

where the ranges include the range of reddening corrections.

We used the "Nebular" software package (Shaw & Dufour 1995) to determine the temperature and density of the gas producing the [N II] and [O III] lines. The allowed values of $\log n_e$ and $\log T_e$ are shown in Figure 9. Both sets of lines must come from regions with high electron densities, $\log n_e > 5.8$, but the temperatures could be fairly low, $\log T_e > 3.85$. One does not normally expect the [N II] and [O III] lines to come from the same volumes of gas because their ionization potentials are so different, but the similarity of their line profiles suggests some overlap of their line formation regions. If so, the temperature and density of the overlap region is given by the overlap area in Figure 9:

$$\begin{aligned} \log n_e &= 6.2 \pm 0.3 \\ \log T_e &= 4.3 \pm 0.2 \end{aligned} \qquad (7)$$

These temperatures and densities are high enough that physical effects not included in the Nebular package could be affecting the line ratios, e.g., radiative and dielectronic recombinations, but the uncertainties introduced by these other effects should be smaller than the large uncertainties introduced by the measurement errors.

Region II: The iron wind is the second thermal region. The wind emits both Fe II and [Fe II] lines, but the forbidden lines are generally quite weak (the 5158 Å line shown in Figure 2 is a rare example of a fairly strong [Fe II] line). The density in the wind is, then, comparable to or greater than the critical density for depopulating the metastable states by collisions. According to Netzer (1988) and Verner et al. (1999) the critical density is $\log n_e \approx 9.5$. Because of this high density, we can also place a meaningful upper limit on the electron temperature in the wind without a detailed treatment of heating and cooling processes. The wind does not produce any Fe III emission lines and, therefore, electron collisions do not ionize a significant fraction of the Fe II atoms to Fe III. From the Saha equation, the kinetic temperature of the boundary between the two stages of ionization is roughly given by $kT_e \sim E_{3,2}/\gamma$ where $E_{3,2}$ is the ionization potential of Fe II and $\gamma = 35.4 - \ln n_e + 1.5 \ln T_e$ (Rybicki & Lightman 1979). Taking $\log n_e = 10$, we find $\gamma \approx 23.5$ and the upper limit to the temperature is $T_e < 8000\ K$. The presence of Fe I lines from the wind (e.g., Multiplet 15) supports this rather low temperature. Conversely, the temperature of the iron wind must be greater than $\sim 7000\ K$ to produce Fe II emission lines (Netzer 1988). Thus, the temperature of the wind is close to $8000\ K$.

In the previous section we found that the local Doppler broadening of the emission lines coming from the wind is 3.1 km s^{-1}. The thermal velocity of iron atoms at $8000\ K$ is about 1.9 km s^{-1}, so all other sources of Doppler broadening, including turbulent velocities and gradients in the expansion velocity, amount to only 2.4 km s^{-1}. The sound speed in gas with a temperature of $8000\ K$ is $\sim$ 9 km s^{-1} so any turbulent flow of gas within the wind is certainly subsonic. There is remarkably little velocity structure to the wind.

We can roughly estimate the mass loss rate $\dot{M}$ in the iron wind from

$$\dot{M} = 4\pi r_w^2 \rho v \approx \left(\frac{L_*}{4\sigma T_w^4}\right)\left(\frac{n_e \mu m_H}{f}\right) v, \qquad (8)$$

where r_w is a characteristic radius from which most of the Fe II emission is coming, ρ is the mass density of the wind, v is the velocity of the wind, L_* is the luminosity of the sgB[e] star, T_w is the temperature of the wind, f is the fraction of hydrogen that is ionized, and the remaining symbols have their usual meanings. We take r_w to be radius where the energy density of the diluted stellar radiation field has an equivalent black body temperature equal to the wind temperature, $4\pi r_w^2 \sigma T_w^4 = L_*/4$. Taking $L_* = 10^5\ L_\odot$, $T_w = 8000\ K$, $\log n_e = 10$, and $v = 32$ km s^{-1}, we find $\dot{M} = 4.4 \times 10^{-7}\ (1/f)\ M_\odot$ yr^{-1}.

Region III: The third thermal region is the source of the strong emission lines of hydrogen and neutral helium.

Most of the helium lines are not suitable for a simple analysis because they are heavily blended and difficult to measure accurately, and they are likely to be optically thick and subject to the effects of radiative transfer. Exceptions are the weak lines at 4713 Å and 5048 Å. Both are 2p-4s transitions, the 5048 Å line in the singlets and the 4713 Å line in the triplets, and should be much less optically thick than the stronger helium lines; and both lines are also relatively uncontaminated by blends. The ratio of their de-reddened intensities is

$$\frac{I(4713)}{I(5048)} \;=\; 3.8 \pm 0.4 \qquad (9)$$

Unfortunately, the very weakness of these lines means the measured line intensities may have substantial internal and external errors, precluding a precise quantitative analysis. Nevertheless, the recombination model and computer program "he5" (Benjamin et al. 1999) suggests that the gas emitting the lines has an electron temperature near $15,000\ K$ with a wide range of possible electron densities centered near $\log n_e = 6$.

The hydrogen Balmer lines have a large decrement. The ratios of their dereddened fluxes at the peaks of the lines are

$$\frac{\mathrm{H}\alpha}{\mathrm{H}\beta} \;=\; 5.3\pm1.3 \quad \text{and} \quad \frac{\mathrm{H}\gamma}{\mathrm{H}\beta} \;=\; 0.35\pm0.03, \qquad (10)$$

which is much steeper than the decrement for Case B recombination ($H_\alpha/H_\beta/H\gamma \approx 2.8/1.0/0.47$). There are two basic ways to produce steep Balmer decrements (Drake & Ulrich 1980). The first is to have a large electron density, $\log n_e \approx 10-12$, so that electrons are excited into the upper levels of the hydrogen atoms by collisions. This mechanism is inconsistent with the densities implied by the helium line ratios. The second is to have a low electron density, $\log n_e < 7$, but a high optical depth to Hα, $\tau_{H\alpha} > 100$, so that Balmer photons are trapped and rapidly degrade to lower members of the Balmer series. This mechanism is consistent with the helium line ratios. We conclude that the steep decrement is produced by high optical depth in Hα.

Region IV: The infrared emission from CI Cam comes from a fourth thermally-distinct region. The infrared emission, which was present before, during, and after the 1998 outburst (Allen 1973; Belloni et al. 1999; Clark et al. 2000), is produced by dust in the circumstellar envelope. The spectral energy distribution of the dust emission has been discussed at length by Belloni et al. (1999) and Clark et al. (2000); here we discuss only the size of the dust shell.

We assume that the infrared emission comes from dust that condenses from the stellar wind when the wind cools below the condensation temperature. Most of the emission comes from the hottest dust near the inner edge of the dusty shell. We assume that this dust has a temperature near $T_{\rm d} = 1350\ K$ and that the inner edge is located at a characteristic distance $r_{\rm shell}$ from CI Cam. If the dust is heated by the sgB[e] star in CI Cam and is in thermal equilibrium, then

$$c\int \mathrm{C_a}(\lambda)\; U_\lambda\; d\lambda \;=\; 4\pi\int \mathrm{C_e}(\lambda)\; B_\lambda(T_{\rm d})\; d\lambda \qquad (11)$$

where c is the speed of light, U_λ is the radiation energy density, and $\mathrm{C_a}(\lambda)$ and $\mathrm{C_e}(\lambda)$ are the absorption and emission cross sections of the dust grains [e.g., Doty & Leung (1994)]. We take $cU_\lambda = 4\pi W B_\lambda(T_*)$, where T_* is the effective temperature of sgB[e] star, W is the geometric dilution factor,

$$W \;=\; \frac{R_*^2}{4r_{shell}^2}, \qquad (12)$$

and R_* is the effective radius of the sgB[e] star. We have, then,

$$W\int \mathrm{C_a}(\lambda)\; B_\lambda(T_*)\; d\lambda \;=\; \int \mathrm{C_e}(\lambda)\; B_\lambda(T_{\rm d})\; d\lambda \qquad (13)$$

We take $\mathrm{C_a} \;=\; \mathrm{C_e} \;=\; \mathrm{C_o}/\lambda^p$, where $p = 0$ corresponds to efficient radiative cooling of the grains and gives a lower limit to r_{shell}; and $p = 1$ corresponds to inefficient cooling and gives an upper limit to the radius. For $p = 0$, equations 12 and 13 yield

$$r_{shell}^2 \;=\; \frac{L_*}{16\pi\sigma T_{\rm d}^4} \qquad (14)$$

and for $p = 1$, they yield

$$r_{shell}^2 \;=\; \frac{L_* T_*}{16\pi\sigma T_{\rm d}^5}. \qquad (15)$$

where L_* is the luminosity of the sgB[e] star. For $L_* = 10^5 L_\odot$ and $T_* = 20,000\ K$, equations 14 and 15 give

$$13 \text{ AU} \ < \ r_{shell} \ < \ 52 \text{ AU}.$$

If the distance to CI Cam is 5 kpc, the angular radius of the shell is between 0.0026 and 0.0104 arcseconds, in agreement with the results of Traub (1999), who found an angular diameter of 0.0052 arcsec in the K band using the IOTA interferometer.

Using the scaling relation from Bjorkman (1998), a spherically symmetric wind can produce dust particles only if the rate of mass loss in the wind is greater than

$$\dot{M} \ > \ 1.7{\times}10^{-7} \left(\frac{r_{shell}}{25 \text{ AU}}\right) \left(\frac{v_\infty}{30 \text{ km s}^{-1}}\right)^2 M_\odot \text{ yr}^{-1}$$

where v_∞ is the wind speed. Adopting $v_\infty = 32$ km s^{-1} and $r_{shell} = 25$ AU, we find $\dot{M} > 1.9 \times 10^{-6} M_\odot$ yr^{-1} in good agreement with the mass loss rate deduced for the Fe II wind if the ionization fraction f is less than ~ 0.1. Unlike Clark et al. (2000), we conclude that the wind need not be episodic nor confined to the equatorial plane of the sgB[e] star.

5. Discussion

The Environment of the Compact Star in CI Cam. The compact star in CI Cam is immersed in a complex environment produced by a two-component wind from the sgB[e] star. One component is a cool, low-velocity wind (the "iron wind"), and the other is a hot, high-velocity wind. The iron wind is dense, $\log n_e > 9.5$, roughly spherical, continuously replenished, and carries away mass at a high rate, $\dot{M} > 10^{-6}\ M_\odot$ yr^{-1}. The wind fills the space around the sgB[e] star and, based on the radius of the inner edge of the infrared-emitting dust shell, it extends to at least 13 AU. The hot, high-velocity wind is the source of the broad H, He, and Na emission lines in the spectrum of CI Cam. This wind has a velocity in excess of 2500 km s^{-1}, a temperature of $1.7{\pm}0.3{\times}10^4\ K$, and a density of $\log n_e \approx 6$.

It is far from clear how the high-velocity and low-velocity winds can co-exist in CI Cam. Other sgB[e] stars also show two-component winds. Typical models for their winds make the low-velocity wind an equatorial outflow, allowing the high velocity wind to escape as a polar outflow. Such models cannot be entirely correct for CI Cam because the low-velocity wind is spherical, not confined to a plane. The high-velocity wind was, however, enhanced and changing rapidly when we observed it. The broad Na D lines present during the outburst were not present before or after the outburst, and although H and He lines are always present, they became much stronger during the outburst (Barsukova et al. 1998; Orlandini et al. 2000; Jaschek & Andrillat 2000). It is possible that the enhanced high-velocity wind may eventually interact with the material in the low velocity wind but had not done so at the time of our observations.

As noted by Belloni et al. (1999) and others, there are similarities between CI Cam and the Be-star X-ray transients. A typical Be-star X-ray transient contains a neutron star in an eccentric orbit that carries it once per orbit through a wind confined to the equatorial plane around the Be star. Enhanced accretion during passage through the equatorial wind causes periodic X-ray outbursts (Bildsten et al. 1997). The outbursts are variable in duration and luminosity. In A0538-66, which has an orbital period of 16.65 days, the outbursts can last from a few hours to 10 days and can have luminosities between 10^{37} and 10^{39} erg s^{-1} (Corbet et al. 1997). The resemblance between CI Cam and the Be-star X-ray transients is only superficial, however. CI Cam is a sgB[e] star, emphatically not a Be star, and its circumstellar material is much denser, far more extended, and much less confined to the equatorial plane than the circumstellar material around a Be star. It is more correct to think of the compact star in CI Cam as continuously burrowing through dense circumstellar material as it orbits the sgB[e] star. The dense environment of the compact star makes CI Cam unique among the known X-ray binaries.

The Peculiarly Low X-ray Luminosity at Quiescence. Because the compact star continuously burrows through the dense wind from the sgB[e] star, accretion is not naturally limited to a short interval of orbital phases as in the Be-star/neutron-star systems. The reverse is true: The compact star should always be accreting at a

high rate, even during quiescence. Let us assume for the moment that the compact star accretes material from the wind at the Bondi accretion rate. For a compact star of mass M_x moving with relative velocity V through a gas with an undisturbed density ρ_∞ and sound speed c_s, the Bondi accretion rate is (Bondi 1952):

$$\dot{M}_x \approx 2\pi\rho_\infty (GM_x)^2 \left(V^2 + c_s^2\right)^{-3/2}. \quad (16)$$

The electron number density in the iron wind is $\log n_e > 9$, so even if the wind is fully ionized, the mass density is greater than $\rho_\infty = 3.3 \times 10^{-15}$ gm cm^{-3}. If the sum of the masses of the two stars is $M_B + M_x = 35M_\odot$ and the semimajor axis of the relative orbit is $a = 0.5$ AU, the orbital period is 2.0×10^6 s and the velocity of the compact star in its relative orbit around the sgB[e] star is 230 km s^{-1}. The iron wind around CI Cam is expanding at 32 km s^{-1}. Adding the wind velocity and the orbital velocity in quadrature, we find $V \approx 230$ km s^{-1} $>> c_s$. If the compact star is a neutron star with a mass $M_x = 1.4M_\odot$, the Bondi accretion rate is then $\dot{M}_x = 6 \times 10^{16}$ gm s^{-1} and the Bondi accretion luminosity is $\dot{E} \approx 7 \times 10^{36}$ erg s^{-1}. If the compact star is a black hole with a mass $M_x = 5M_\odot$, the accretion rate is $\dot{M}_x = 8 \times 10^{17}$ gm s^{-1} and the accretion luminosity is $\dot{E} \approx 4 \times 10^{37}$ erg s^{-1}. The luminosity scales as $a^{3/2}$.

The Bondi accretion luminosity differs greatly from the observed quiescent X-ray luminosity, $L(2 - 10$ keV$) = 5 \times 10^{32}$ (d/5 kpc)^2 erg s^{-1}. The fundamental reason for the high luminosity is the large capture radius for Bondi accretion:

$$r_{cap} \approx \frac{2GM_x}{V^2}. \quad (17)$$

For the example at hand, $r_{cap} = 0.05$ AU for a $1.4M_\odot$ neutron star and $r_{cap} = 0.17$ AU for a $5M\odot$ black hole. Some process either prevents the compact star from accreting at the Bondi rate or prevents the accretion energy from being emitted at X-ray energies. Whatever the process, it cannot rely on a fine tuning of parameters to prevent the X-ray emission because the material in the circumstellar envelope has a wide range of temperatures, densities, and velocities.

The Nature of the Compact Star and the Source of the Outburst. The most direct ways a neutron star can betray itself is through Type I bursts, which are caused by a thermonuclear runaway in the envelope of a neutron star, or through type II bursts or periodic modulations of the X-ray light curve, which require a magnetized neutron star. None of these has been observed in CI Cam. Even quasi-periodic oscillations are absent. Belloni et al. (1999) have suggested that periodicities from a neutron star could be smeared or obliterated by strong absorption or scattering of the X-rays, but the X-ray spectrum is inconsistent with strong absorption or scattering. Thus, there is no direct evidence for a neutron star in CI Cam.

Although there is likewise no direct evidence for a black hole, the high X-ray luminosity of CI Cam during outburst, $L(2 - 25$ keV$) > 3.0 \times 10^{38}$ erg s^{-1}, and the large ratio of its quiescent to peak luminosities, $L_q/L_p < 1.7 \times 10^{-6}$, do provide indirect evidence for a black hole. Figure 10 is a modified version of similar figures in Narayan et al. (1997) and Garcia et al. (1998). The figure plots L_q/L_p against L_p for the X-ray novae in which the compact star has been positively identified as a neutron star or black hole. The systems with neutron stars are shown as open circles and those with black holes are shown as filled circles. With only one exception the black holes systems have higher peak luminosities than the neutron star systems, and with only one possible exception the ratio of quiescent to peak luminosities of the black hole systems is smaller than the that of the neutron stars systems. With *no* exceptions the neutron star systems are confined to the upper left quadrant of the figure and are fully segregated from the black hole systems.

Narayan et al. (1997) and Garcia et al. (1998) originally proposed two reasons for the segregation. First, black holes have higher peak luminosities because they are more massive than neutron stars and have higher Eddington luminosities. Second, any residual accretion onto a black hole during quiescence is swallowed by the event horizon and produces little X-ray emission, whereas residual accretion onto a neutron star hits the surface of the neutron star and does produce emission. The real reasons for the segregation are likely to be more complicated (Menou et al. 1999) but the empirical fact remains that neutron stars and black holes are segregated in the figure.

CI Cam is also plotted in Figure 10. We have adopted a peak luminosity corresponding to a distance of 5 kpc, the lower limit to the true luminosity, and a luminosity ratio corresponding to all the quiescent luminosity coming from the compact star, an upper limit to the true ratio. Even taking these limits, CI Cam falls within the region occupied by the black holes and outside the region occupied by the neutron stars. Figure 10 is, of course, circumstantial evidence for a black hole, not proof, but the evidence is strong enough to make CI Cam a good candidate for a black hole binary.

We speculate that the X-ray outburst of CI Cam was caused by the same mechanism responsible for the outbursts of X-ray novae, that is, by an instability in the accretion disk around the compact star (Lasota 2001). We further speculate that the reason the outburst was so short is that the accretion disk in CI Cam is smaller than the accretion disks in other X-ray novae because the disk is fed from a stellar wind, not by Roche-lobe overflow. The rate of decline of a disk-instability outburst should scale by the viscous time scale in the disk,

$$\tau \;=\; \frac{r}{v_r} \;\propto\; r^{7/5}, \tag{18}$$

where v_r is the velocity at which matter drifts radially inward due to viscosity (Frank et al. 1992). The exponent on r corresponds to electron scattering opacity, which is more appropriate than free-free opacity for the outburst state. The outburst of CI Cam decayed on an e-folding time scale between 0.6 and 2.3 days; in contrast, the Fast Rise Exponential Decay (FRED) outbursts of X-ray novae generally have decay timescales between 10 and 50 days (Chen et al. 1997). Equation 18 implies that the disk in CI Cam is 5 to 20 times smaller than the disks in more typical X-ray transients.

The radius of an accretion disk produced by Roche-lobe overflow should should be about 1/4 of the separation of the stars. We take A0620-00 and V404 Cyg as typical X-ray novae with FRED outbursts and with accretion disks maintained by Roche-lobe overflow. Their orbital periods are 0.323 d and 6.46 d respectively, and the radii of their accretion disks should be roughly 6×10^{10} cm and 60×10^{10} cm. The disk in CI Cam should be 5 to 20 times smaller than these disks.

Wind accretion can produce the smaller disk in CI Cam. The radius of an accretion disk maintained by wind accretion is given roughly by the circularization radius,

$$r_{circ} \;=\; \frac{G^3 M_x^3\, \omega^2}{V^8}, \tag{19}$$

where $\omega \approx 2\pi/P_{orb}$ and P_{orb} is the orbital period of the compact star (Frank et al. 1992). For the example of the previous section $P_{orb} = 2.04 \times 10^6$ s and $V = 230$ km s^{-1}, yielding $r_{circ} \approx 7.9 \times 10^8$ cm for a $1.4M_\odot$ neutron star, and $r_{circ} \approx 3.6 \times 10^{10}$ cm for a $5M_\odot$ black hole. Despite the large exponent on V, r_{circ} scales only linearly with the semi-major axis of the relative orbit.

Thus, unless the mass of the compact star is significantly greater than $5M_\odot$ or the semi-major axis of its orbit is greater than 0.5 AU, the size of the wind-fed accretion disk is small enough to account for the short outburst.

Finally, we note that the black hole binary V4641 Sgr also had anomalously-short but high-luminosity X-ray outbursts. The orbital period of V4641 Sgr is 2.8 days and the secondary star in the system is an evolved B-type star with a mass between 5.5 and $8.1M_\odot$ (Orosz et al. 2001). The black hole in this system could also be accreting via a small disk that is fed by a wind or a focused wind from the B star instead of a stream through the inner Lagrangian point.

6. Summary

We obtained high dispersion spectroscopy of CI Cam, the optical counterpart of XTE J0421+560, two weeks after the peak of its short outburst in 1998 April. The salient results from the observations are:

1. CI Cam is a sgB[e] star. Its spectrum has a blue continuum with strong, broad emission lines of H, He, and Na that were greatly enhanced during the outburst. It also has a thicket of weak, narrow emission lines of neutral and singly ionized metals, and even narrower lines of [N II] and [O III]. There are no absorption lines in the visual spectrum other than interstellar absorption features.

2. Based on the ultraviolet continuum between 1150 Å and 2700 Å, the reddening and ex-

tinction are $E(B-V) = 0.85 \pm 0.05$, $A_V = 2.3 \pm 0.3$, and $R_V = 2.7 \pm 0.2$.

3. CI Cam is more distant than previously supposed. Its spectroscopic properties place it among the most luminous supergiant B[e] stars and imply a distance greater than 5 kpc. The radial velocity of CI Cam with respect to the Local Standard of Rest, -51 km s^{-1}, and its galactic coordinates, $(l,\ b) \approx (149°,\ 4°)$, also imply a distance greater than 5 kpc.

4. The X-ray luminosity at the peak of the outburst was $L(2\!-\!25\,\mathrm{keV}) \approx 3.0\!\times\!10^{38}$ erg s^{-1} for a distance of 5 kpc, making CI Cam one of the most luminous X-ray transients. The ratio of quiescent luminosity to peak luminosity in the 2 – 25 keV band is $L_q/L_p < 1.7 \times 10^{-6}$.

5. The sgB[e] star emits a two-component wind. One component is a cool, low-velocity wind (the "iron wind"), which is dense, $\log n_e > 9.5$, roughly spherical, continuously replenished, and has been present since at least 1931. The mass loss rate due to the wind is high, $\dot{M} > 10^{-6}\ M_\odot$ yr^{-1}. The wind fills the space around the sgB[e] star and, from the size of the infrared-emitting dust shell, extends to a radius between 13 AU and 50 AU. The second component is a hot, high-velocity wind, which is the source of the broad H, He, and Na emission lines in the spectrum of CI Cam. This wind has a velocity in excess of 2500 km s^{-1}, a temperature of $1.7 \pm 0.3 \times 10^4\ K$, and an electron number density of $\log n_e \approx 6$. It is unclear how the high-velocity and low-velocity winds can co-exist.

6. Although the compact star in CI Cam is immersed in the dense circumstellar wind from the sgB[e] star, it burrows through the wind while producing only a small fraction, $< 10^{-4}$, of the X-ray emission expected from the Bondi accretion rate except for rare transient outbursts. This picture, a compact star traveling in a wide orbit through the dense circumstellar envelope of a sgB[e] star, occasionally producing transient X-ray outbursts, makes CI Cam unique among the known X-ray binaries.

7. The lack of type I and type II bursts, the lack of periodic X-ray pulsations, the great luminosity at the peak of the outburst, and the large ratio of peak to quiescent luminosity is circumstantial evidence that the compact object in CI Cam is a black hole, not a neutron star.

8. We speculate that the outburst of CI Cam was caused by the same disk instability mechanism responsible for the outbursts of X-ray novae. The reason the outburst was so short is that the accretion disk in CI Cam is smaller than the accretion disks in other X-ray novae because the disk is fed from a stellar wind, not by Roche-lobe overflow.

We thank H. Dinerstein, R. Hynes, Z. Ioannou, A. King, G. Shields for useful discussions. Support for proposal #8138 was provided by NASA through a grant from the Space Telescope Science Institute, which is operated by the Association of Universities for Research in Astronomy, Inc., under NASA contract NAS 5-2655.

Table 1
Identified Lines in the Spectrum of CI Cam

Permitted Lines		Forbidden Lines	
Species	Example	Species	Example
H	Balmer series	[N II]	5755 Å
He I	5876 Å	[O I]	6300 Å
He II	4686 Å	[O III]	4959/5007 Å
C I	Multiplet 3	[Fe II]	5158 Å
N I	Multiplet 1		
O I	8446 Å		
Na II	D lines		
Mg I	Multiplet 2		
Si II	Multiplet 5		
Ca II	IR triplet		
Sc II	Multiplet 29		
Ti II	Many		
Cr II	Many		
Fe I	Multiplet 15		
Fe II	Many		

Table 2
The Kinematic Properties of the Circumstellar Environment

	Region I	Region II	Region III
Typical lines	[N II], [O III]	Metal lines Paschen lines	Balmer lines He I, Na D
Half Width at Half Max	16 km s^{-1}	32 km s^{-1}	50 – 85 km s^{-1}
Line Profiles	Roughly Gaussian	Weak lines rectangular; Strong lines asymmetric Gaussians	Asymmetric; Blue wings to -2500 km s^{-1} Red wings to $+1000$ km s^{-1}

Table 3
The Thermal Properties of the Circumstellar Environment

	Region I	Region II	Region III	Region IV
Source of:	Highly forbidden lines	Metal lines	Balmer & He I lines	Infrared continuum
Velocity (km s^{-1})	16	32	Up to 2500	...
Temperature (K)	...	8000	$(1.7 \pm 0.3) \times 10^4$	1350 K
$\log n_e$ (cm^{-3})	>6.0	> 9.5	≈ 6	...

REFERENCES

Allen, D. A. 1973, MNRAS, 161, 145

Barsukova, E. A., Fabrika, S. N., Pustilnik, S. A., & Ugryumov, A. V. 1998, Bull. Spec. Astrophys. Obs., 45, 147

Belloni, T., et al. 1999, ApJ, 527, 345

Benjamin, R. A., Skillman, E. D., & Smits, D. P. 1999, ApJ, 514, 307

Bergner, Yu. K. et al. 1995, A&AS, 112, 221

Bildsten, L. et al. 1997, ApJS, 113, 367

Bjorkman, J. E. 1998, in "B[e] Stars", ed. by A. M. Hubert & C. Jaschek (Dordrecht: Kluwer Acad. Pub.) p. 189

Blitz, L., Fich, M., & Stark, A. A. 1982, ApJS, 49, 183

Bondi, H. 1952, MNRAS, 112, 195

Burton, W. B. 1988a, in Galactic and Extragalactic Radio Astronomy, ed. by G. L. Verschuur & K. I. Kellermann (New York: Springer-Verlag) p. 295

Burton, W. B. 1988b, in The Outer Galaxy, ed. by L. Blitz & F. J. Lockman (Berlin: Springer-Verlag) p. 94

Cardelli, J. A., Geoffrey, C. C., & Mathis, J. S. 1989, ApJ, 345, 245

Chan, G., & Fich, M. 1995, AJ, 109, 2611

Chen, W., Shrader, C. R., & Livio, M. 1997, ApJ, 491, 312

Clark, J. S. et al. 2000, A&A, 356, 50

Corbet, R. H., Charles, P. A., Southwell, K. A., & Smale, A. P. 1997, ApJ, 476, 833

Dame, T. M. et al. 1987, ApJ, 322, 706

Doty, S. D., & Leung, C. M. 1994, ApJ, 424, 729

Downes, R. A. 1984, PASP, 96, 807

Drake, S. A., & Ulrich, R. K. 1980, ApJS, 42, 351

Frank, J., King, A., & Raine, D. 1992, Accretion Power in Astrophysics (Cambridge: Cambridge Univ. Press)

Frontera, F. et al. 1998, A&A, 339, L69

Garcia, M. R., McClintock, J. E., Narayan, R., & Callanan, P. J. 1998, in Wild Stars in the Old West, ASP Conf. Series, 137, 506

Grandi, S. A. 1975, ApJ, 196, 465

Harmon, B. A., Fishman, G. J., & Paciesas, W. S. 1998, IAU Circ., 6874

Hjellming, R. M., & Mioduszeswki, A. J. 1998a, IAU Circ., 6857

Hjellming, R. M., & Mioduszeswki, A. J. 1998b, IAU Circ., 6872

Hynes, Robert I. 1998, private communication

Ikeda, Y., Kawabata, K. S., & Akitaya, H. 2000, A&A, 355, 256

Jaschek, C. 1998, in B[e] Stars, ed. A. M. Hubert & C. Jaschek (Dordrecht: Kluwer), 27

Jaschek, C., & Andrillat, Y. 2000, in IAU Col. No. 175, The Be Phenomenon in Early-Type Stars, ASP Conf. Series, 214, 83

Kastner, S. O., & Bhatia, A. K. 1995, ApJ, 439, 346

Kerr, F. J., Bowers, P. F., Kerr, M., & Jackson, P. D. 1986, ApJS, 66, 373

Krełowski, J., & Schmidt, M. 1997, ApJ, 477, 209

Lamers, H. J. G. L. M., Zickgraf, F.-J., de Winter, D., Houziaux, L., & Zorec, J. 1998, A&A, 340, 117

Lasota, J.-P. 2001, New Astron. Rev., 45, 449

Menou, K. et al. 1999, ApJ, 520, 276

Merrill, P. W. 1933, ApJ, 77, 44

Miroshnichenko, A. S. 1995, A&AT, 6, 251

Miroshnichenko, A. S. 1998, in B[e] Stars, ed. A. M. Hubert & C. Jaschek (Dordrecht: Kluwer), 145

Napiwotzki, R., 1993, Acta Astron., 43, 415

Narayan, R., Garcia, M. R., & McClintock, J. E. 1997, ApJ, 478, L79

Neckel, T., Klare, G., & Sarcander, M. 1980, A&AS, 42, 251

Netzer, H. 1988, in IAU Coll. 94, Physics of Formation of Fe II Lines Outside LTE, ed. R. Viotti, A. Vittone, & M. Friedjung (Dordrecht: Reidel), 247

Orlandini, M., et al. 2000, A&A, 356, 163

Orosz, J. E. et al. 2001, ApJ, 555, 489

Osterbrock, D. E., Fulbright, J. P., & Bida, T. A. 1997, PASP, 109, 614

Oudmaijer, R. D., Proga, D., Drew, J. E., & de Winter, D. 1998, MNRAS, 300, 170

Pacheco, J. A. De Freitas 1998, in B[e] Stars, ed. A. M. Hubert & C. Jaschek (Dordrecht: Kluwer), 221

Paciesas, W. S., & Fishman, G. J. 1998, IAU Circ., 6856

Predehl, P., & Schmitt, J. H. M. M. 1995, A&A, 293, 889

Revnivtsev, M., Emelyanov, A., & Borozdin, K. 1999, Astron. Lett., 25, 296

Robinson, E. L., Welsh, W. F., Adams, M. T., & Cornell, M. E. 1998, IAU Circ., 6862

Rybicki, G. P., & Lightman, A. P. 1979, Radiative Processes in Astrophysics (New York: Wiley).

Sciortino, S. et al. 1990, ApJ, 361, 621

Shaw, R. A., & Dufour, R. J. 1995, PASP, 107, 896

Smith, D. & Remillard, R. 1998, IAU Circ., 6855

Taylor, J. H., & Cordes, J. M. 1993, ApJ, 411, 674

Tobin, W. 1985, A&A, 142, 189

Traub, W. A. 1999, private communication.

Tull, R. G., MacQueen, P. J., Sneden, C., & Lambert, D. L. 1995, PASP, 107, 251

Ueda, Y., Ishida, M., Inoue, H., Dotani, T., Greiner, J. & Lewin, W. H. G. 1998, ApJ, 508, L167

Verner, E. M., Verner, D. A., Korista, K. T., Ferguson, J. W., Hamann, F., & Ferland, G. J. 1999, ApJS, 120, 101

Wagner, R. M., & Starrfield, S. G. 1998, IAU Circ., 6857

Zickgraf, F.-J., Wolf, B., Stahl, O., Leitherer, C., & Klare, G. 1985, A&A, 143, 421

Zickgraf, F.-J., Wolf, B., Stahl, O., Leitherer, C., & Appenzeller, I. 1986, A&A, 163, 119

Zickgraf, F.-J. 1998, in "B[e] Stars", ed. by A. M. Hubert & C. Jaschek (Dordrecht: Kluwer Acad. Pub.) p. 1

Zorec, J. 1998, in B[e] Stars, ed. A. M. Hubert & C. Jaschek (Dordrecht: Kluwer), 27

Figure Captions

Fig. 1.— The spectrum of CI Cam from 5825 Å to 5910 Å. The He I line at 5876 Å has an equivalent width of 110 ± 15 Å and broad asymmetric wings extending further to the blue than the red. The Na D lines at 5890/96 Å are cut by at least two complexes of interstellar absorption. The spectrum is magnified in the lower panel to show the full extent of the blue wing on the He I line, which extends to at least 5845 Å (–1500 km s^{-1}), and the myriad of weak metal lines. The weak absorption at 5850 Å is a diffuse interstellar absorption band.

Fig. 2.— The spectrum of CI Cam from 5125 Å to 5205 Å with identifications for the more prominent emission lines. Although the strongest lines in this region of the spectrum come from permitted Fe II, lines of Ti II, Mg I are also present. Lines of [Fe II] are generally weak in the spectrum of CI Cam; the lines at 5158.0/58.8 Å are rare examples of fairly strong lines.

Fig. 3.— The spectrum of CI Cam from 8380 Å to 8510 Å. The strongest lines are the O I line at 8446 Å and the Ca II line at 8498 Å, one of the calcium infrared triplet lines. The spectrum is magnified in the lower panel to show the Paschen lines. The Paschen lines can be identified to P34 in the next order of the echelle spectrogram.

Fig. 4.— The spectrum of CI Cam from 8590 Å to 8725 Å. The strongest line is the Ca II line at 8662 Å, a member of the calcium infrared triplet. The spectrum is magnified in the lower panel to show the weaker lines in the spectrum, notably the N I lines from multiplets 1 and 8, the P14 line of hydrogen, and both permitted and forbidden lines of Fe II.

Fig. 5.— The lower panel is the observed, heavily extincted, ultraviolet spectrum of CI Cam. The original spectrograms have been rebinned into 15 Å bins in the short wavelength region and 20 Å bins in the long wavelength region. The upper pannel shows the de-extincted spectrum of CI Cam with the spectrum of BD+33°2642 overplotted for comparison. The residual differences between the CI Cam spectrum and the BD+33°2642 spectrum are all due to real features in the CI Cam spectrum: Fe II emission between 2300 Å and 2500 Å and wind features at shorter wavelengths, for example.

Fig. 6.— The highly forbidden lines of [O III] at 5007 Å and [N II] at 5754 Å. The half width at half maximum of both lines is 16 km s^{-1}; the [N II] line also has broad wings extending to ±5 Å (±260 km s^{-1}).

Fig. 7.— The solid line is the observed spectrum of CI Cam from 5416 Å to 5436 Å. The lines of Ti II, Cr II, and Fe I are symmetric and rectangular with a pronounced flat top; the Fe II lines are more rounded and have asymmetric wings. The half width at half maximum of all the lines is close to 32 km s^{-1}. The dashed line is the spectrum produced by a model in which each line is the convolution of a rectangular profile and a line broadening profile – a narrow Gaussian for the lines of Ti II, Cr II, and Fe I, plus a second broader gaussian for the Fe II lines to represent their asymmetric wings.

Fig. 8.— The Hα and Hβ lines of hydrogen in CI Cam. The equivalent width of Hα is $\sim 750 \pm 50$ Å and that of Hβ is 73 ± 3 Å. The spectra are magnified in the lower panel to show the wings of the lines. The blue wing of Hα extends to at least 6510 Å (–2400 km s^{-1}) and the blue wing of Hβ to 4845 Å (–1000 km s^{-1}).

Fig. 9.— The locus of points in the $(\log n_e,\ \log T_e)$ plane corresponding to the [O III] (the dashed lines) and [N II] (the solid lines) emission line ratios. The upper line of each pair corresponds to a reddening of $E(B-V) = 1.1$ and the lower line corresponds to $E(B-V) = 0.65$.

Fig. 10.— The outburst luminosities of X-ray novae and their luminosity ranges between outburst and quiescence. Neutron star systems are denoted by open circles, black hole systems by small filled circles, and CI Cam by the large filled hexagon. The downward pointing arrows denote systems for which the quiescent flux has not been measured. CI Cam is plotted at an outburst luminosity corresponding to a distance of 5 kpc, the lower limit to the true luminosity. The neutron star systems are confined to the upper left quadrant of the figure; CI Cam is in the lower right quandrant where most of the black hole systems are located.

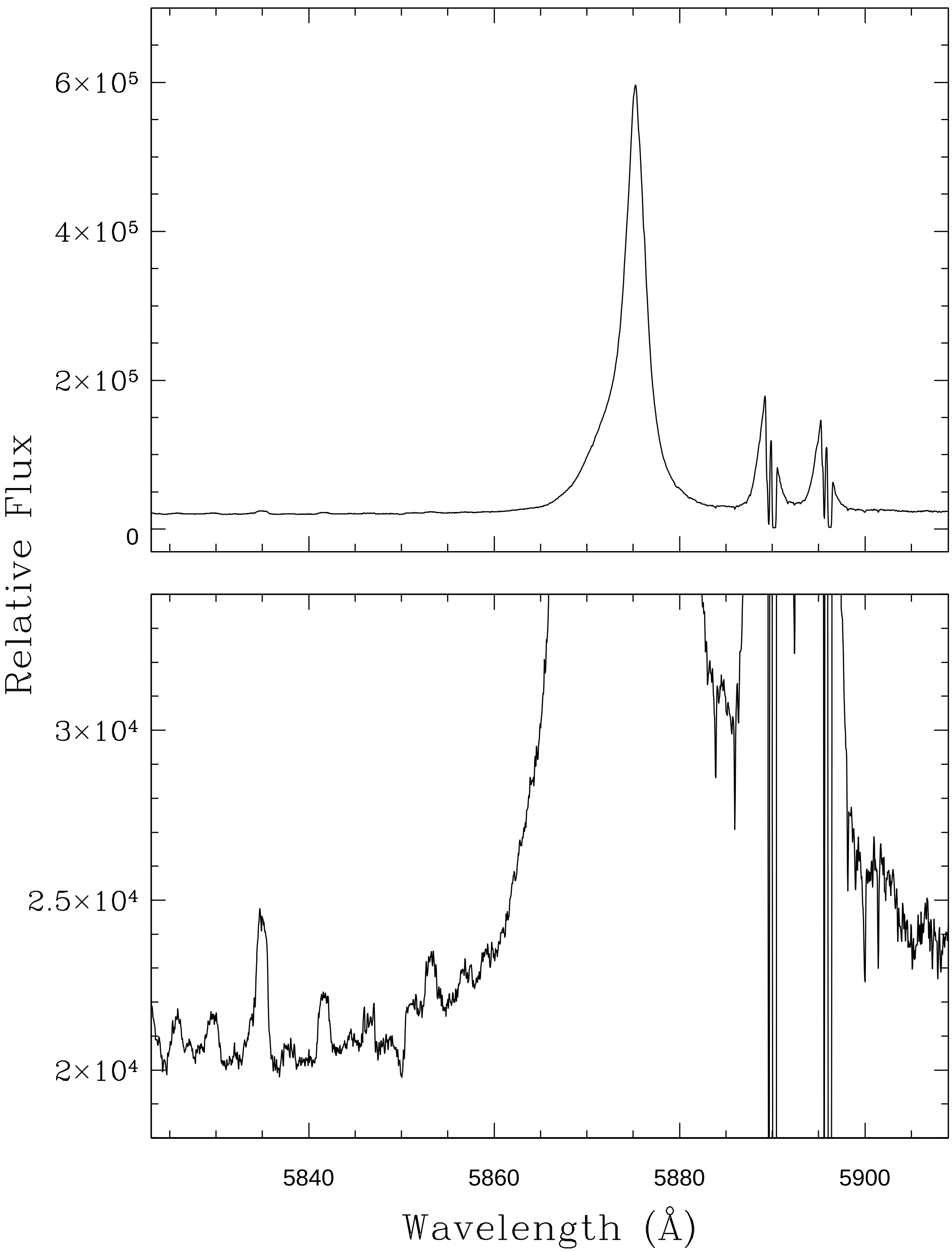
6×10⁵
4×10⁵
2×10⁵
0
Relative Flux
3×10⁴
2.5×10⁴
2×10⁴
5840
5860
5880
5900
Wavelength (Å)

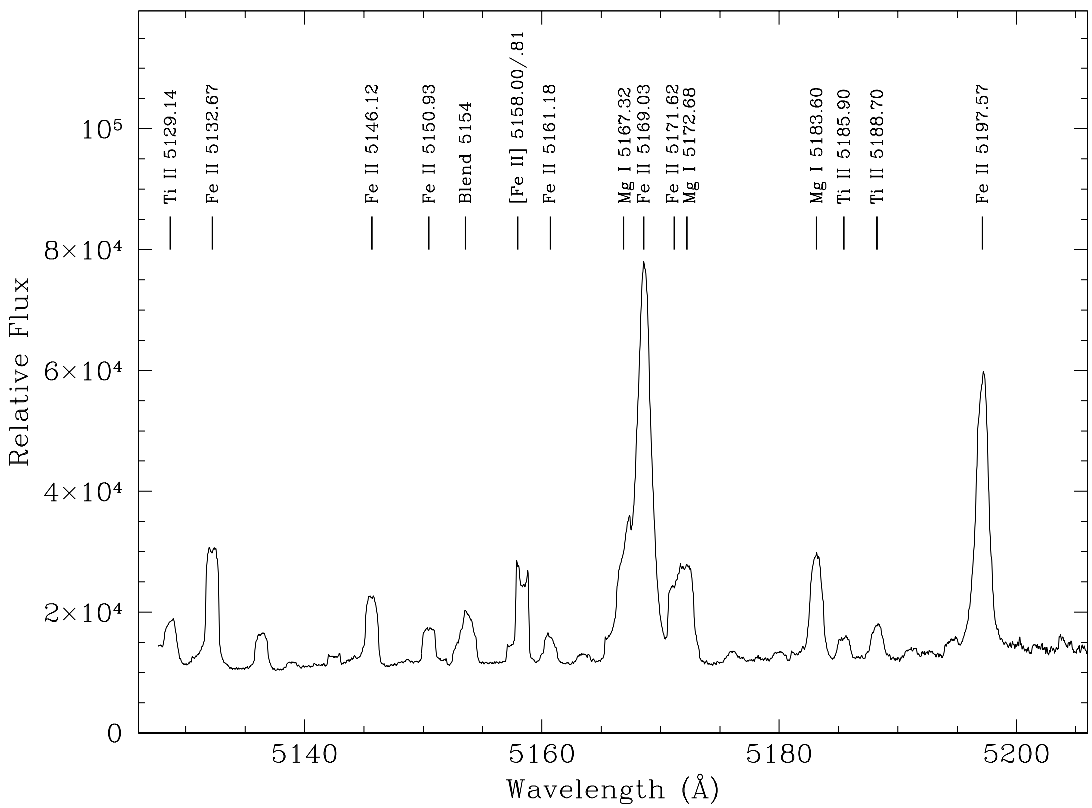

Ti II 5129.14
Fe II 5132.67
Fe II 5146.12
Fe II 5150.93
Blend 5154
[Fe II] 5158.00/.81
Fe II 5161.18
Mg I 5167.32
Fe II 5169.03
Fe II 5171.62
Mg I 5172.68
Mg I 5183.60
Ti II 5185.90
Ti II 5188.70
Fe II 5197.57
Relative Flux
Wavelength (Å)
0
2×10⁴
4×10⁴
6×10⁴
8×10⁴
10⁵
5140
5160
5180
5200

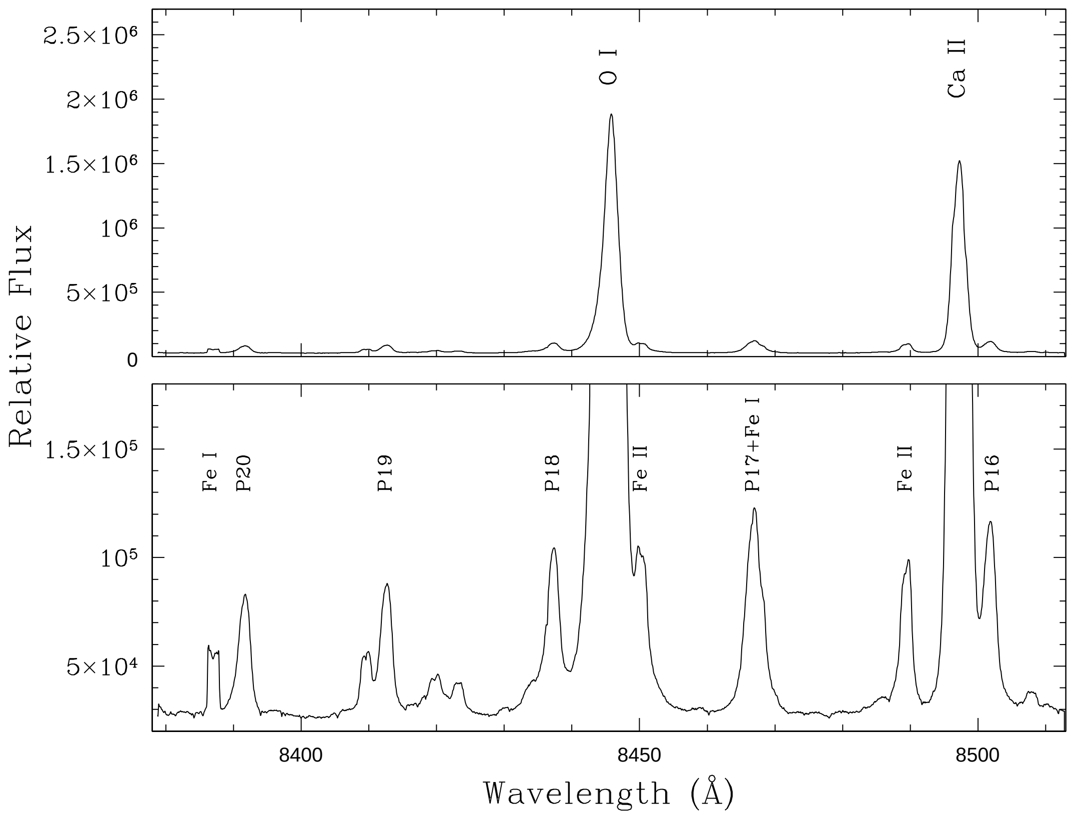

2.5×10^6
2×10^6
1.5×10^6
10^6
5×10^5
0
O I
Ca II
1.5×10^5
10^5
5×10^4
Fe I
P20
P19
P18
Fe II
P17+Fe I
Fe II
P16
8400
8450
8500
Relative Flux
Wavelength (Å)

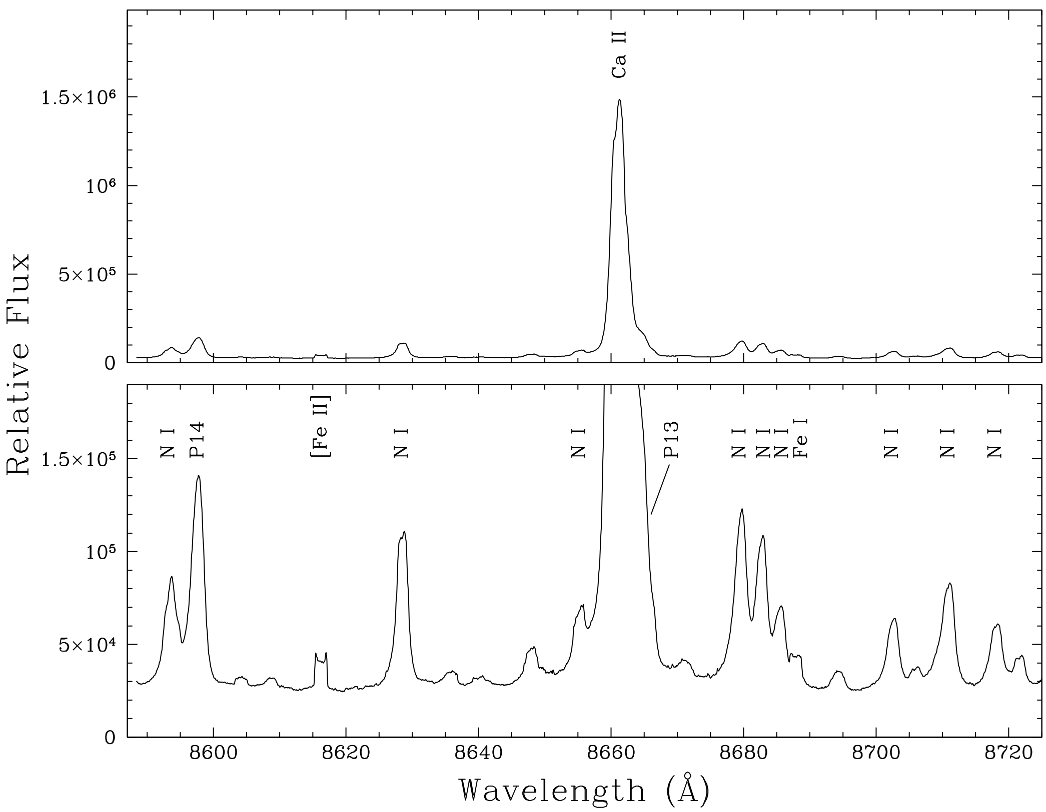

Ca II
1.5×10⁶
10⁶
5×10⁵
0
Relative Flux
N I
P14
[Fe II]
N I
N I
P13
N I
N I
N I
Fe I
N I
N I
N I
1.5×10⁵
10⁵
5×10⁴
0
8600
8620
8640
8660
8680
8700
8720
Wavelength (Å)

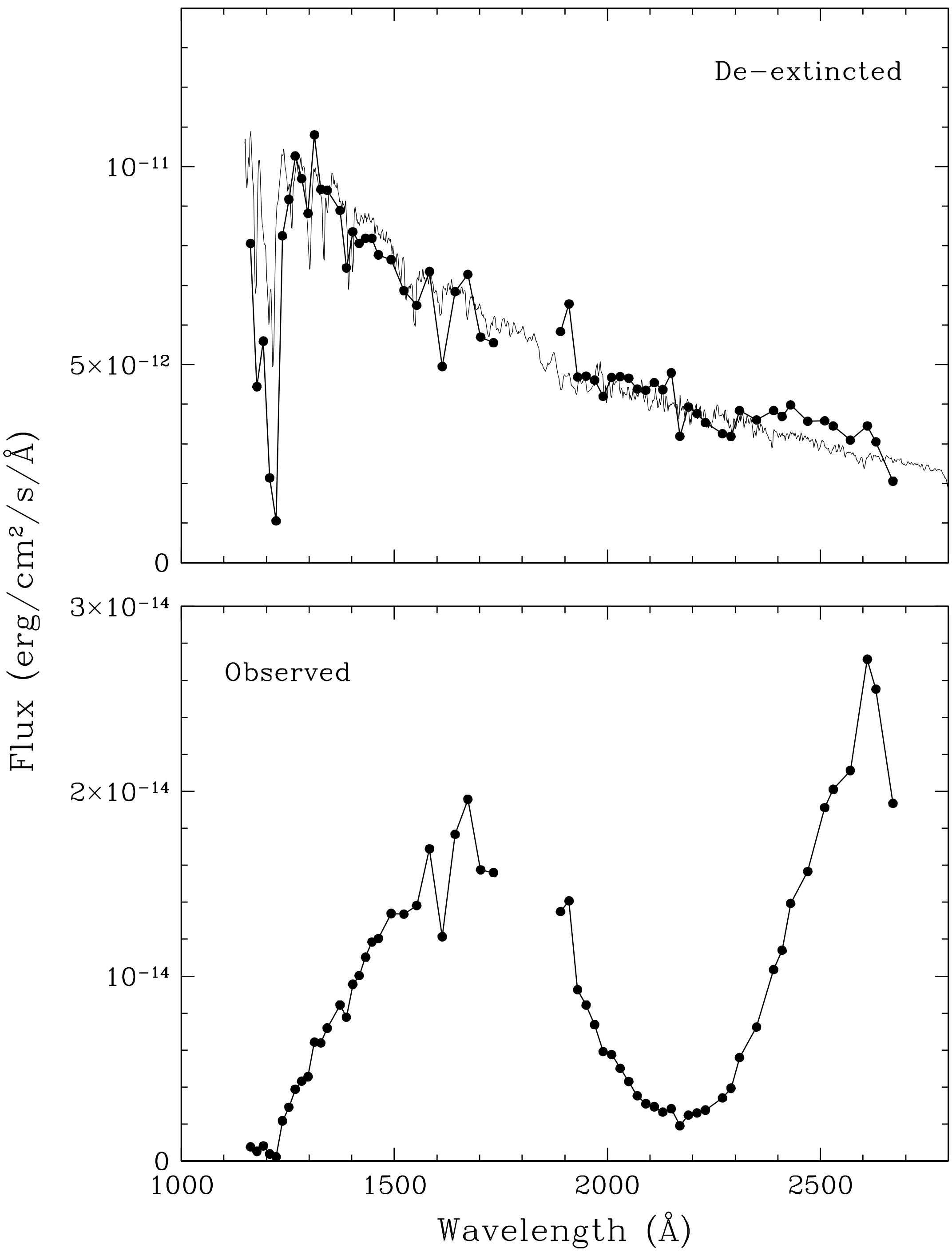
De-extincted
Observed
Flux (erg/cm²/s/Å)
Wavelength (Å)
10^{-11}
5×10^{-12}
0
3×10^{-14}
2×10^{-14}
10^{-14}
0
1000
1500
2000
2500

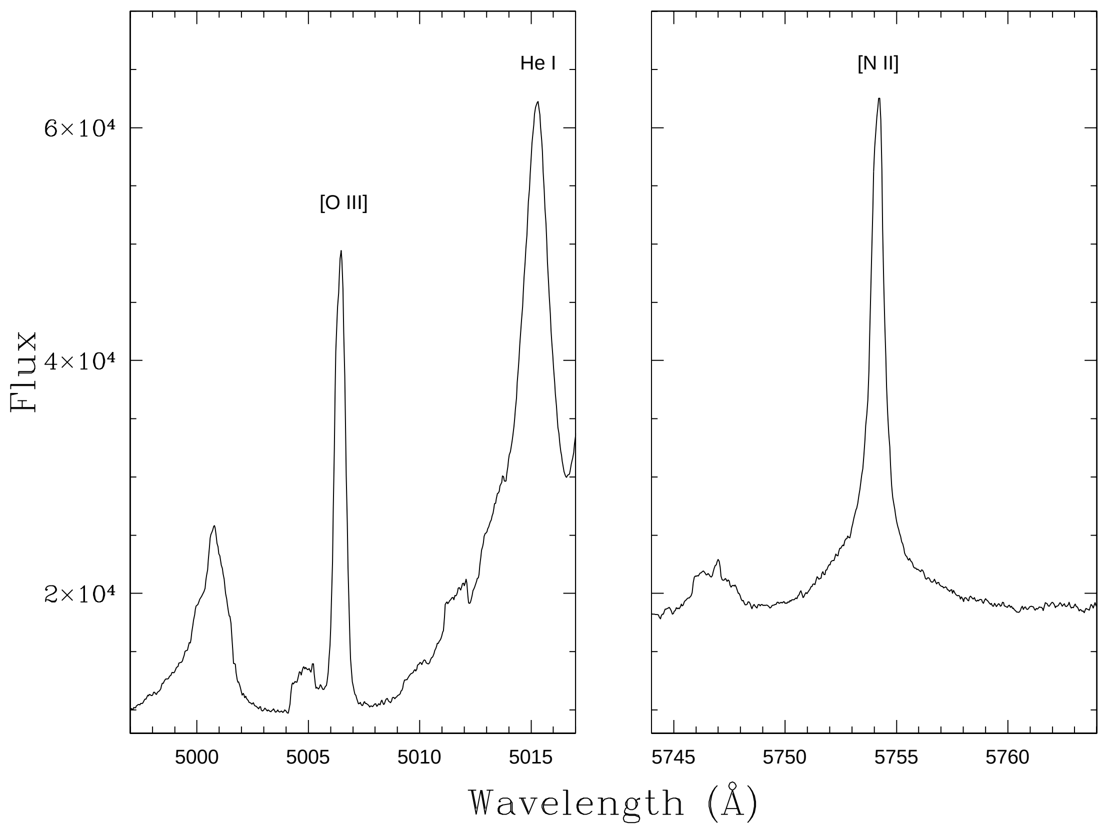

He I
[O III]
[N II]
Flux
6×10⁴
4×10⁴
2×10⁴
5000
5005
5010
5015
5745
5750
5755
5760
Wavelength (Å)

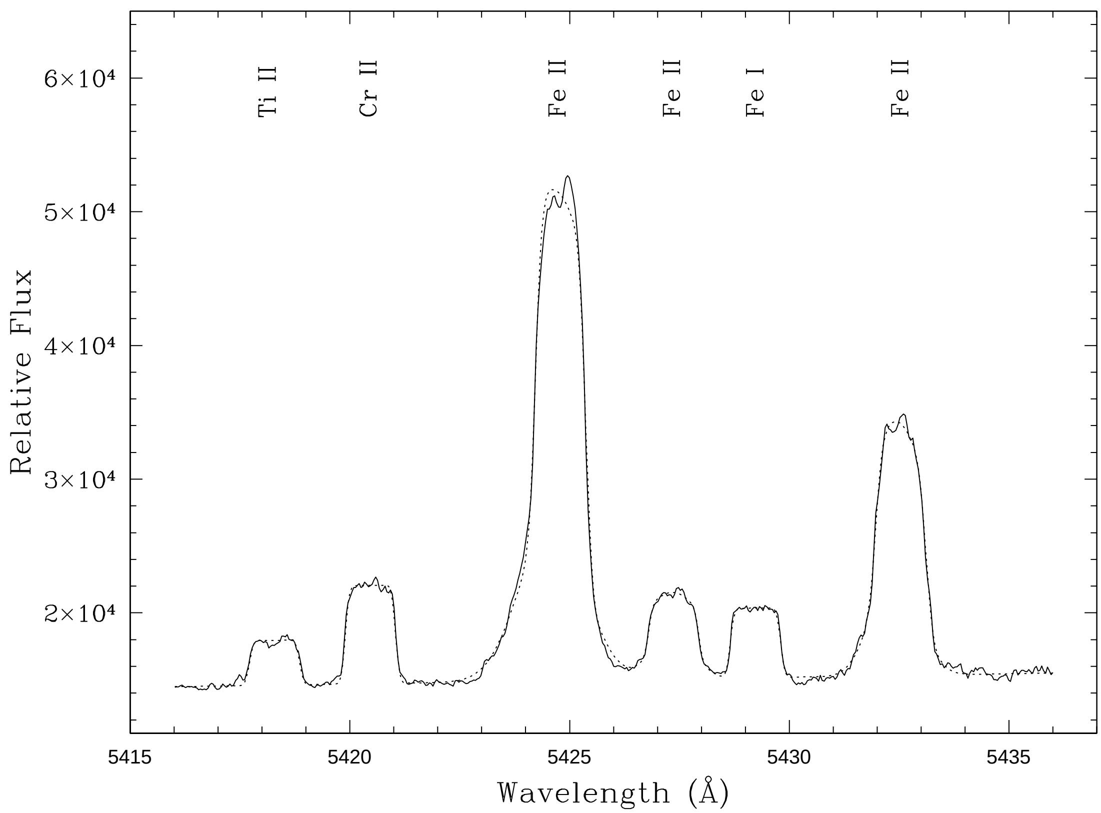

Ti II
Cr II
Fe II
Fe II
Fe I
Fe II
Relative Flux
6×10⁴
5×10⁴
4×10⁴
3×10⁴
2×10⁴
5415
5420
5425
5430
5435
Wavelength (Å)

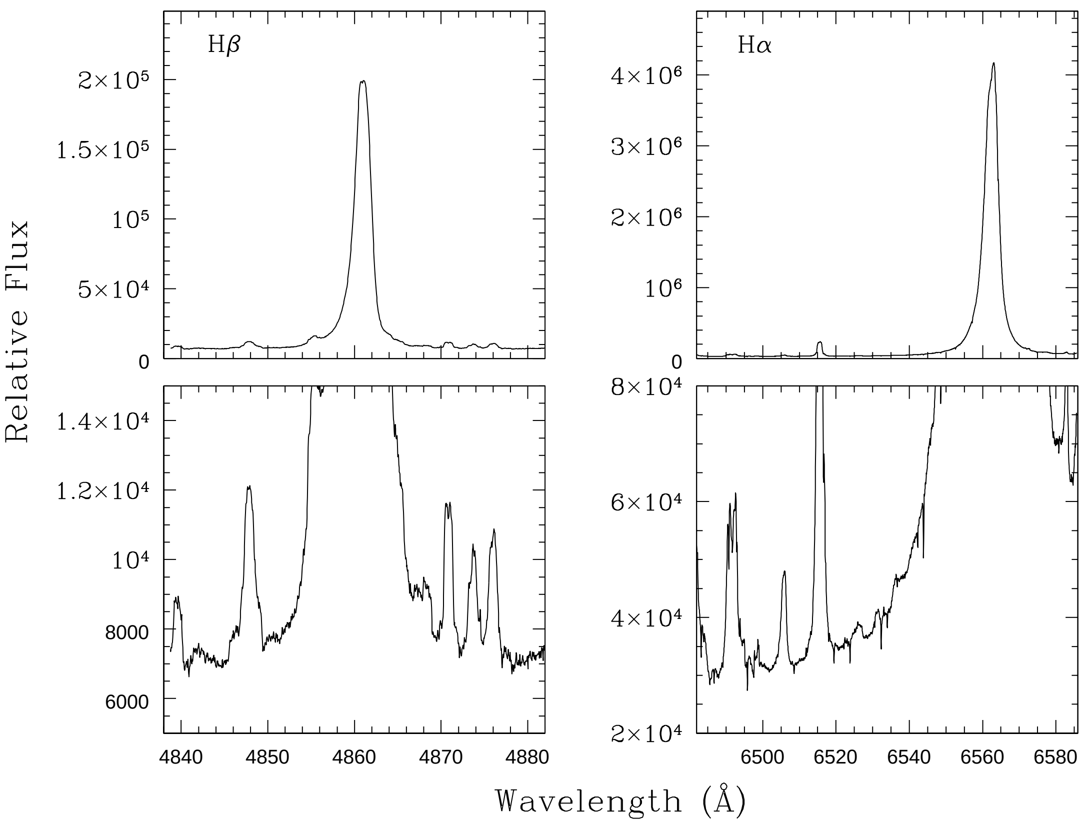

Hβ
Hα
Relative Flux
Wavelength (Å)
2×10⁵
1.5×10⁵
10⁵
5×10⁴
0
4×10⁶
3×10⁶
2×10⁶
10⁶
0
1.4×10⁴
1.2×10⁴
10⁴
8000
6000
8×10⁴
6×10⁴
4×10⁴
2×10⁴
4840
4850
4860
4870
4880
6500
6520
6540
6560
6580

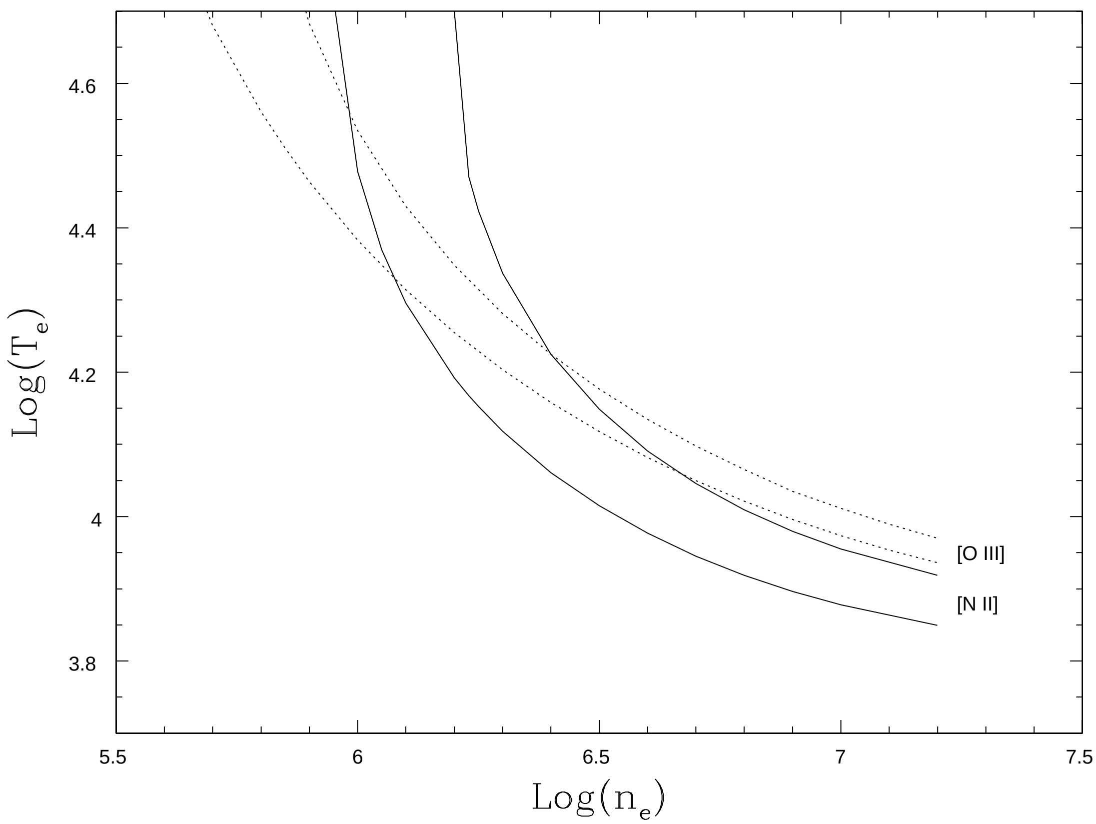

Log(T_e)
4.6
4.4
4.2
4
3.8
5.5
6
6.5
7
7.5
Log(n_e)
[O III]
[N II]

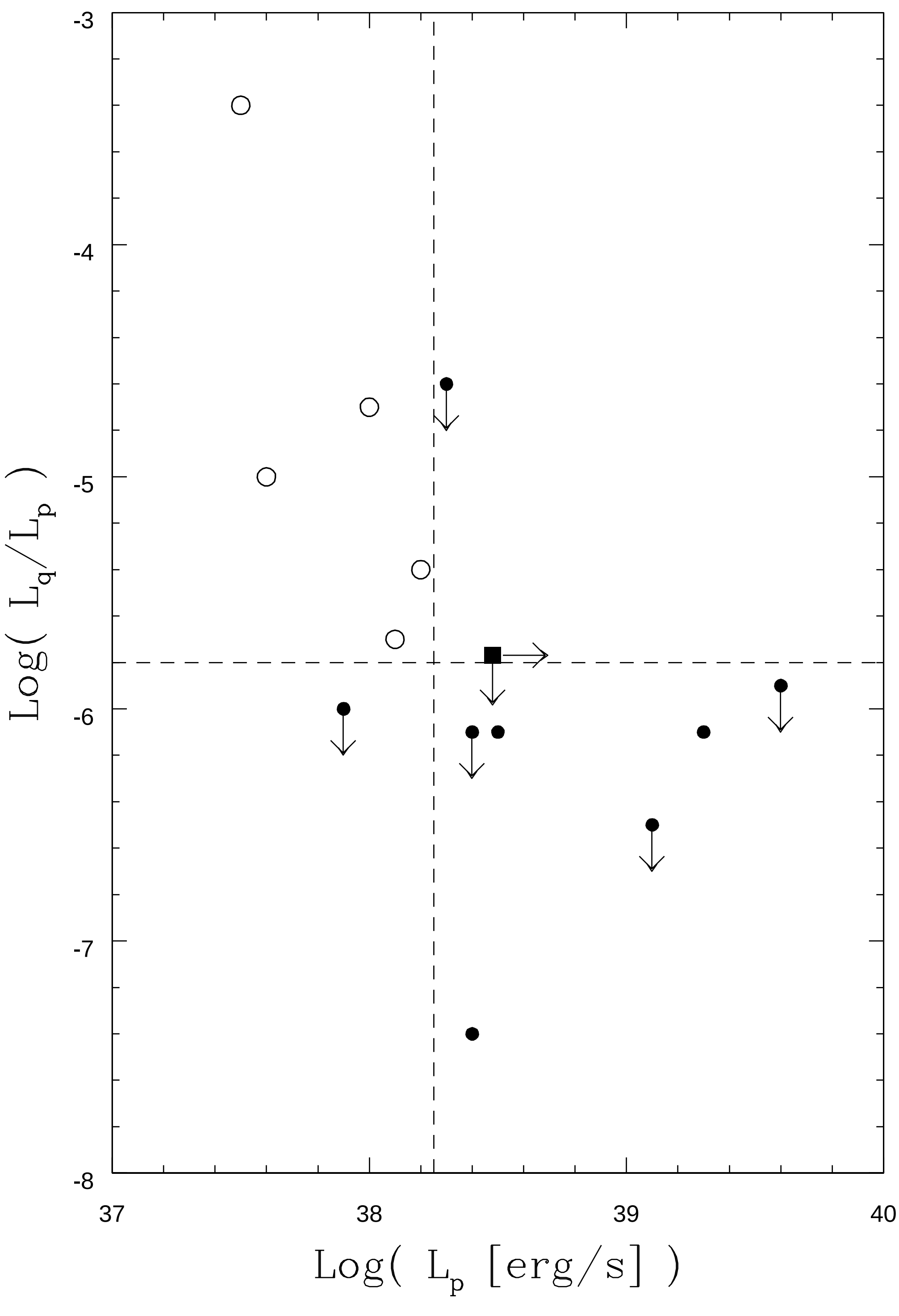

-3
-4
-5
-6
-7
-8
37
38
39
40
Log(L_q/L_p)
Log(L_p [erg/s])